Electrochimica Acta 56 (2011) 8285–8290

Contents lists available at ScienceDirect

Electrochimica Acta

journal homepage: www.elsevier.com/locate/electacta

Spherical clusters of β-Ni(OH)$_2$ nanosheets supported on nickel foam for nickel metal hydride battery

Ying Wang, Dianxue Cao, Guiling Wang*, Shasha Wang, Jiyan Wen, Jinling Yin

Key Laboratory of Superlight Material and Surface Technology of Ministry of Education, College of Material Science and Chemical Engineering, Harbin Engineering University, Harbin, 150001, PR China

ARTICLE INFO

Article history:
Received 9 March 2011
Received in revised form 28 June 2011
Accepted 28 June 2011
Available online 6 July 2011

Keywords:
Nickel hydroxide
Nanosheet
Spherical cluster
Nickel foam
Nickel metal hydride battery

ABSTRACT

Spherical clusters of Ni(OH)$_2$ nanosheets are directly grown on skeletons of nickel foam via a facile template-free spontaneous growth method. The obtained electrode (β-Ni(OH)$_2$/Ni-foam) is characterized by X-ray diffractometry, scanning and transmission electron microscopy and thermal analysis. Results show that Ni(OH)$_2$ has a β-phase structure and presents on the nickel foam skeleton mostly as spherical clusters with a diameter of ~10 μm. The spheres are composed of nanosheets with thickness of ~60 nm, width of ~230 nm and length up to ~2 μm, and the nanosheets are assembled by nanoparticles with diameter of ~20 nm. The electrochemical performance of the β-Ni(OH)$_2$/Ni-foam electrode is evaluated by cyclic voltammetry and galvanostatic charge–discharge tests. The difference between the oxygen evolution reaction onset potential and the anodic peak potential for this electrode (~100 mV) is larger than that for β-Ni(OH)$_2$ nanosheets and nanotubes powder electrode (~65–77 mV) and much larger than that for commercial spherical β-Ni(OH)$_2$ powder electrode (~25–47 mV), indicating that the β-Ni(OH)$_2$/Ni-foam electrode can be fully charged. The specific discharge capacity of β-Ni(OH)$_2$ in the β-Ni(OH)$_2$/Ni-foam electrode reaches 275 mAh g^{-1}, which is close to the theoretical value, lower than that of β-Ni(OH)$_2$ nanotubes (315 mAh g^{-1}), but higher than that of nanosheets (219.5 mAh g^{-1}), commercial micrometer grade spherical powders (265 mAh g^{-1}) and microtubes (232.4 mAh g^{-1}).

1. Introduction

Nickel metal hydride (Ni–MH) rechargeable batteries have high specific energy, high specific power, long cycling life, and superior safety. They are competitive power sources for all-electric plug-in vehicles and hybrid vehicles [1]. However, when Ni–MH batteries are frequently charged and discharged at high rates or high temperatures, their performances are reduced due to capacity fading, increase of internal resistance and decrease of cycle stability [2]. It is generally recognized that the performance of a Ni–MH battery is mainly limited by properties of the positive electrode, i.e. Ni(OH)$_2$ electrode. During charge and discharge processes, solid-state proton intercalation/deintercalation reactions take place at the Ni(OH)$_2$ electrode where both electrons and protons are exchanged; this leads to continuous changes in both composition and phase structure of the electrode active materials [1,3].

The charge and discharge reactions of a nickel hydroxide electrode in alkaline electrolytes are usually considered to be a one-electron process involving oxidation and reduction between β-Ni(OH)$_2$ and β-NiOOH and can be simply described as:

$$\beta\text{-Ni(OH)}_2 + \text{OH}^- \rightleftharpoons \beta\text{-NiOOH} + \text{H}_2\text{O} + \text{e}^- \quad (1)$$

This reaction mechanism involves an equivalent proton diffusion through solid-state lattices of β-Ni(OH)$_2$ and β-NiOOH [4]. Therefore, the specific charge–discharge capacity of β-Ni(OH)$_2$ depends on the magnitude of the resistance for the transportation of equivalent protons within the solid lattices as well as the electronic conductivity of Ni(OH)$_2$, particularly at high charge and discharge rates. Decreasing the particle size and changing the morphology of Ni(OH)$_2$ have been proved to be effective ways for reducing the resistance of equivalent proton transportation [5–9]. Nanostructured Ni(OH)$_2$ particles with various morphologies that have been recently prepared by different methods, indeed exhibit improved capacity and cycling reversibility. These nano-sized Ni(OH)$_2$ particles include nanorods, nanowires, nanotubes, nanoribbons, and nanosheets [10–17]. However, nano-sized Ni(OH)$_2$ particles are generally prepared in a powder form and need to be pressed onto a current collector (e.g. nickel foam) with conducting additives (e.g. carbon black) and binders to obtain the electrode. This conventional electrode preparation procedure may lead to the reduction of utilization efficiency of active materials due to ineffective contact between Ni(OH)$_2$ particles and the

* Corresponding author. Tel.: +86 451 82589036; fax: +86 451 82589036.
E-mail address: wangguiling@hrbeu.edu.cn (G. Wang).

0013-4686/$ – see front matter © 2011 Elsevier Ltd. All rights reserved.
doi:10.1016/j.electacta.2011.06.098

current collector. The addition of ancillary materials also decreases the specific energy of electrodes. Moreover, these conventional electrodes lack buffer ability in response to volume change of the active material particularly when overcharged.

In this study, spherical clusters of $Ni(OH)_2$ nanosheets were directly grown onto nickel foam current collector via a template-free self-growth method, and the obtained electrode, free of conducting additives and binders, was evaluated as the positive electrode of the Ni–MH battery. Even though nano-structured Co_3O_4, $Ni_xCo_yO_4$ and CuO have been grown on Si wafer, Ti foil or Ni foam substrates by the template-free growth method used in this work, the grown of $Ni(OH)_2$ nanosheets on Ni foam has not been reported in literatures as far as we know.

2. Experimental

2.1. Preparation and characterization of clusters of $Ni(OH)_2$ nanosheets

Clusters of $Ni(OH)_2$ nanosheets attached on nickel foam were prepared via a template-free growth method [18–21]. 10 mmol $Ni(NO_3)_2$ and 6 mmol NH_4NO_3 were dissolved in 35 cm^3 H_2O + 15 cm^3 ammonia (30 wt%). The solution was magnetically stirred for 10 min at room temperature and heated at 90 ± 1 °C for 2 h (growth ready solution). Nickel foam (10 mm × 10 mm × 1.1 mm, 110 PPI, 320 g m^{-2}, Changsha Lyrun Material Co., Ltd. China) was degreased with acetone, etched with 6.0 mol dm^{-3} HCl for 10 min, rinsed with water, soaked in 0.1 mmol dm^{-3} $NiCl_2$ solution for 4 h, and thoroughly rinsed again with water. The pretreated nickel foam was immersed in the growth solution for 12 h at 90 ± 1 °C for the growth of nanosheets. The above-mentioned condition was the optimized growth condition, and we found that the morphology, amount, specific capacity and cycling stability of $Ni(OH)_2$ strongly depend on the growing time. For example, shorter growing time results in an uneven coverage of $Ni(OH)_2$ on Ni foam and longer growing time leads to the formation of thicker $Ni(OH)_2$ film on Ni foam, which tends to peels off during charge–discharge cycling. After growth, the electrode was thoroughly washed with H_2O and calcined at 250 °C for 2 h in air. The obtained electrode has a $Ni(OH)_2$ loading of 7 mg cm^{-2}.

The morphology was examined by scanning electron microscope (SEM, JEOL JSM-6480) and transmission electron microscope (TEM, FEI Teccai G2 S-Twin, Philips). The structure was analyzed using X-ray diffractometer (XRD, Rigaku TTR III) with Cu Kα radiation (λ = 0.1514178 nm). The 2θ ranges from 10° to 90° with a scan rate of 5° min^{-1} and a step width of 0.01°. Thermo-gravimetric and differential thermal analysis (TG/DTA) were performed with a Pyris-Diamond thermal analyzer (PerkinElmer) in a flow of air (40 cm^3 min^{-1}) at a heating rate of 20 °C min^{-1} from room temperature to 800 °C in an Al_2O_3 sample pan.

2.2. Electrochemical measurements

Electrochemical measurements were performed in a conventional three-electrode electrochemical cell using a computerized potentiostat (Autolab PGSTAT302, Eco Chemie) controlled by GPES software. The $Ni(OH)_2$/Ni-foam acted as the working electrode. A blackened Pt gauze was employed as the counter electrode. A saturated calomel electrode (SCE) served as the reference. 6 mol dm^{-3} KOH + 0.625 mol dm^{-3} LiOH solution was used as the electrolyte. The addition of LiOH into the electrolyte is to diminish the possible detrimental effect of the iron impurity [22]. All potentials were referred to the SCE reference electrode and all electrochemical measurements were performed at room temperature. The solutions were made with analytical grade chemical reagents and Milli-Q water (18 MΩ cm, Millipore). Prior to each measurement, the working electrode was soaked in the electrolyte for 12 h at ambient temperature.

2.3. Ni–MH battery tests

A Ni–MH battery was assembled with $Ni(OH)_2$/Ni-foam positive electrode and AB_5-type hydrogen storage alloy negative electrode. To prepare the negative electrode, the hydrogen storage alloy powder, $MmNi_{4.03}Co_{0.42}Mn_{0.31}Al_{0.24}$ (Dandong Hongyuan alloy Co. Ltd. China), was mixed with polytetrafluoroethylene (PTFE) emulsion and sodium carboxymethylcellulose (CMC) colloid to obtain a paste (mass ratio: $MmNi_{4.03}Co_{0.42}Mn_{0.31}Al_{0.24}$:PTFE:CMC = 8:1:1). The mixture was then smeared onto a Ni-foam sheet with a point-welded nickel wire as current collector, dried at 70 °C for 2 h and pressed under a pressure of 7 MPa. The electrode was then soaked in the electrolyte for 24 h prior to use. The capacity of the hydrogen storage alloy electrode is 30 wt% more than the $Ni(OH)_2$/Ni-foam electrode. Both electrodes have the same geometrical area of 1.0 cm^2 (10 mm × 10 mm). The sandwich of positive electrode/polypropylene membrane/negative electrode was squeezed between two Plexiglas blocks and immersed in 6 mol dm^{-3} KOH + 0.625 mol dm^{-3} LiOH solution. Constant current charge/discharge tests were performed on a battery test system (Land CT2001A, Wuhan Jinnuo, China) at room temperature.

3. Results and discussion

3.1. Characterization of β-$Ni(OH)_2$/Ni-foam electrode

Fig. 1 shows the XRD patterns of the $Ni(OH)_2$ powders scratched from nickel foam. The XRD pattern matches well with the standard crystallographic spectrum of hexagonal β-$Ni(OH)_2$, with a space group of $P3m_1$ (JCPDS card No. 14-0117), and with no peaks detected from other phases. The lattice constants are calculated to be $a = b = 0.3123$ nm, $c = 0.4610$ nm. These values are closely consistent with the standard values ($a = b = 0.3126$ nm, $c = 0.4605$ nm, JCPDS 14-0117) of β-$Ni(OH)_2$ in the range of errors. The XRD results therefore indicate that particles grown on nickel foam are pure phase β-$Ni(OH)_2$. The broad XRD lines indicate the nano-crystalline nature of the material. The average crystallite sizes, estimated using Scherrer's relationship based on the half width of the [1 0 1] peak, are ca. 23 nm.

Fig. 2 shows the SEM images of β-$Ni(OH)_2$ coated on nickel foam and TEM images of β-$Ni(OH)_2$ powder scratched from Ni foam skeleton. The SEM image at low resolution (Fig. 2a) shows

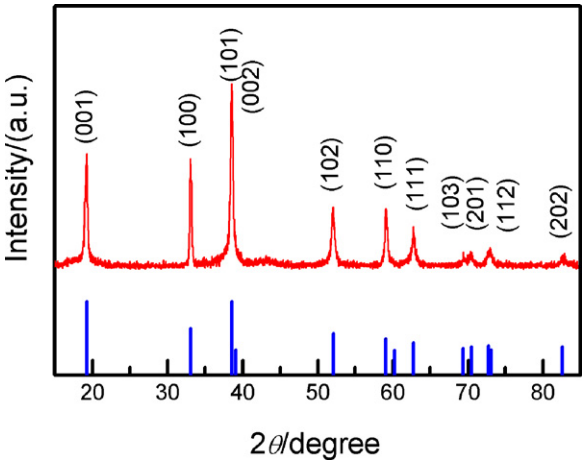

Fig. 1. XRD patterns of $Ni(OH)_2$ powder scratched down from the nickel foam.

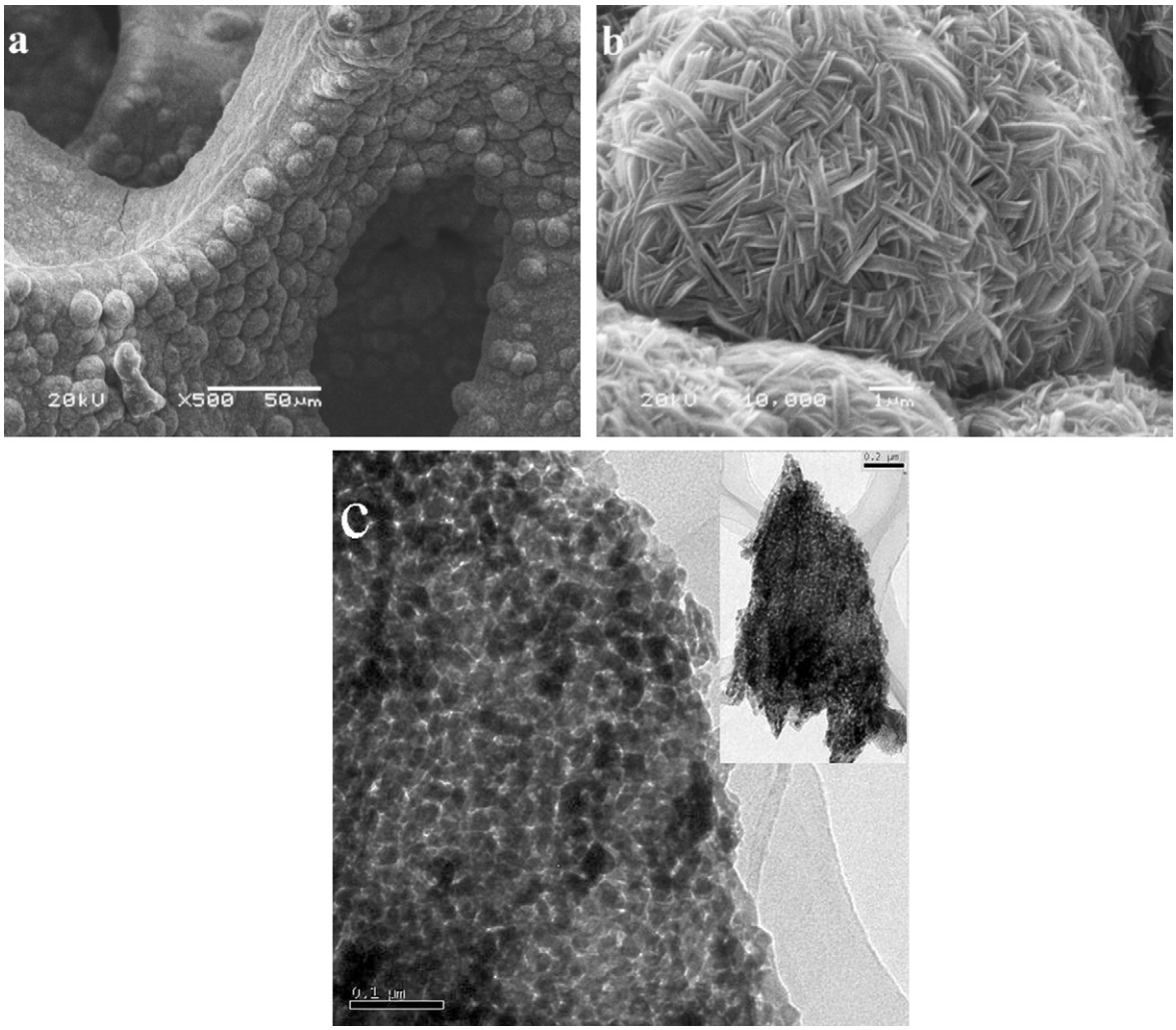

Fig. 2. SEM images of $Ni(OH)_2$ attached on nickel foam skeleton (a and b) and the TEM image of a single nanosheet scratched down from the nickel foam (c).

that β-$Ni(OH)_2$ presents on the nickel foam skeleton mostly as spherical clusters, which have relatively uniform size with a diameter of ~10 μm. High resolution SEM image (Fig. 2b) indicates that β-$Ni(OH)_2$ spheres are actually composed of nanosheets (or nanoribbons) with thickness of ~60 nm, width of ~230 nm and length up to ~2 μm. The TEM image (Fig. 2c) demonstrates that β-$Ni(OH)_2$ nanosheets are composed of nanoparticles with diameter of ~20 nm, which is consistent with XRD results. This unique structure of nanosheets provides β-$Ni(OH)_2$ with a large surface area and porous structure, which facilitates high rate charge and discharge due to the following reasons: (1) the interspaces between neighboring nanoparticles and nanosheets will allow easy diffusion of the electrolyte and to buffer the volume change caused by the transformation between β-$Ni(OH)_2$ and γ-NiOOH during charge–discharge process [23,24]. This volumetric change may lead to poor electric contact between the current collector and β-$Ni(OH)_2$/γ-NiOOH, and accordingly cause rapid capacity decay during electrochemical charge–discharge cycles. (2) The porosity combined with the small particle size will enhance the contact area between β-$Ni(OH)_2$ and electrolyte, and shorten proton diffusion length.

The thermal decomposition behavior of the β-$Ni(OH)_2$/Ni-foam electrode (the Ni foam weight is 30 mg) prior to calcination was investigated by thermal analysis. The TG–DTA curves are shown in Fig. 3. Two weight loss steps can be seen. The first stage (25–250 °C) with a weight loss of ~2% can be assigned to the evaporation of water, ammonia and nitrate anions adsorbed on the surface and trapped in intercrystallite pores. The second stage consists of a rapidly weight loss region (250–325 °C) and a relatively slow weight loss region (325–550 °C). The total weight loss in the second stage is ~21%, which is close to the theoretical value of 19.4% for the decomposition of $Ni(OH)_2$ to NiO. The DTA curve shows an endothermic peak with a maximum located at 314 °C. In the second stage, the temperature range of the endothermic peak in the DTA curve matches well with that of weight loss in the TG curve.

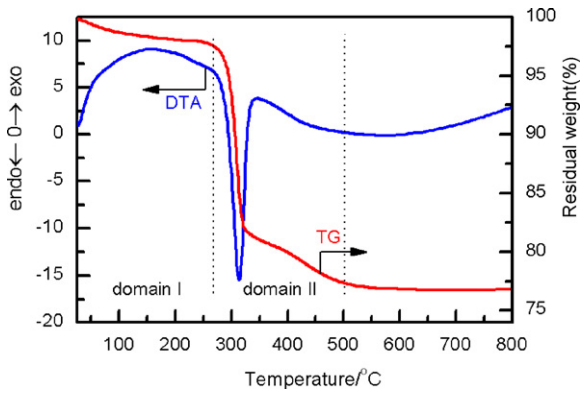

Fig. 3. TG–DTA curves of $Ni(OH)_2$/Ni-foam electrode.

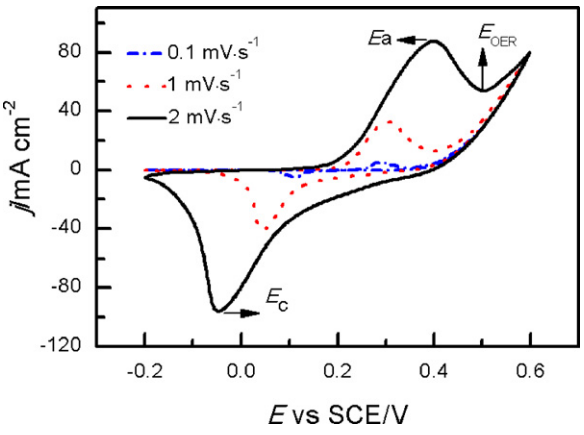

Fig. 4. Cyclic voltammograms of $Ni(OH)_2$/Ni-foam electrode at different scan rates between 0.1 and 2 mV s^{-1}.

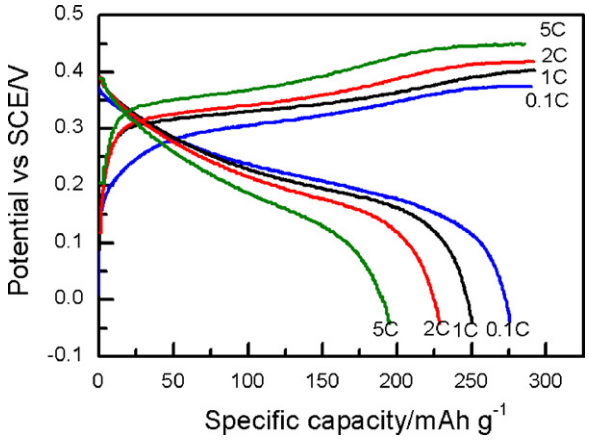

Fig. 5. Discharge curves of the $Ni(OH)_2$/Ni-foam electrode measured at different discharge rates.

Accordingly, the second weight loss region can be attributed to decomposition of $Ni(OH)_2$ to NiO [11,25,26].

3.2. Electrochemical performance of the $Ni(OH)_2$/Ni-foam electrode

Fig. 4 shows the cyclic voltammograms (CV) of β-$Ni(OH)_2$/Ni-foam electrode. The profile of the CV is typical for β-$Ni(OH)_2$ in alkaline medium and is in good agreement with that reported in literatures [7,12,25,27–29], i.e. only one pair of well-defined anodic/cathodic peak was observed, which can be attributed to the redox reaction of $Ni(OH)_2$/NiOOH couple (Eq. (1)). In general, the difference between the anodic (E_a) and cathodic (E_c) peak potentials is a measure of the reversibility of the redox reaction, and the difference between the onset potential (E_{OER}) for oxygen evolution reaction (OER) and the anodic peak potential (E_a) is an important parameter for judging the performance of the electrode. E_a, E_c, E_{OER}, $E_a - E_c$, and $E_{OER} - E_a$ taken from Fig. 4 for our β-$Ni(OH)_2$/Ni-foam electrode are summarized in Table 1. The potential difference ($E_a - E_c$) between the anodic and cathodic peaks becomes larger with the increase of scan rate, demonstrating the quasi-reversible nature of the redox couple. Cai et al. [12] and Li et al. [29] reported that $E_a - E_c$ is around 120–130 mV for β-$Ni(OH)_2$ nanotube power electrode and ~180 mV for commercial micrometer grade spherical β-$Ni(OH)_2$ powder electrode at a scan rate of 0.5 mV s^{-1}. Shangguan et al. [7] found that $E_a - E_c$ for non-spherical β-$Ni(OH)_2$ micro-powder electrode is 202 mV at a scan rate of 1 mV s^{-1}. The $E_a - E_c$ for our β-$Ni(OH)_2$/Ni-foam electrode is 175 and 260 mV at 0.1 and 1 mV s^{-1} scan rate, respectively. So our β-$Ni(OH)_2$/Ni-foam exhibits larger $E_a - E_c$ than commercial spherical β-$Ni(OH)_2$ powder electrode and β-$Ni(OH)_2$ nanotube powder electrode. The large peak potential separation is possibly due to low electronic conductivity of the $Ni(OH)_2$ layer because, unlike conventional $Ni(OH)_2$ powder electrode, no conducting additives (such as carbon black) were used in the β-$Ni(OH)_2$/Ni-foam electrode. The value of $E_{OER} - E_c$ for the β-$Ni(OH)_2$/Ni-foam electrode is about 100 mV and is nearly independent of the scan rate (Table 1).

Table 1
Numerical values of the CV.

Scan rate (mV s^{-1})	Potentials (mV)				
	E_a	E_c	E_{OER}	$E_a - E_c$	$E_{OER} - E_a$
0.1	288	113	395	175	107
1	303	43	403	260	100
2	398	-47	504	445	106

E vs. SCE.

This value is larger than carnation-like β-$Ni(OH)_2$ and $Ni(OH)_2$ nanotubes (~65–77 mV) and much larger than commercial spherical β-$Ni(OH)_2$ powder (~25–47 mV) [12,28]. The large potential separation allows the β-$Ni(OH)_2$/Ni-foam electrode to be fully charged (i.e. complete oxidation of Ni^{2+} to Ni^{3+}) before oxygen evolution.

Fig. 5 shows the discharge curves of β-$Ni(OH)_2$/Ni-foam electrode at different discharge rates. The newly prepared electrode exhibits an open circuit potential of −0.297 V vs. SCE. According to Eq. (1), the theoretical specific capacity of $Ni(OH)_2$ is 289 mAh g^{-1}. The specific discharge capacity of the β-$Ni(OH)_2$ in our β-$Ni(OH)_2$/Ni-foam electrode reaches 275 mAh g^{-1} at 0.1 C discharge rate, which is close to the theoretical value, and remains to be 195 mAh g^{-1} at 5 C, demonstrating that the electrode has high specific capacity and superior rate performance comparing to commercial micrometer grade spherical β-$Ni(OH)_2$ powders. Notably, the actual charge–discharge reactions taking place in the $Ni(OH)_2$ electrode are quite complex. It has been reported that four polymorphs of nickel hydroxides and oxyhydroxides, namely, β-$Ni(OH)_2$, β-NiOOH, γ-NiOOH, and α-$Ni(OH)_2$, can exist in the charge–discharge process. γ-NiOOH contains tetravalent nickel (Ni^{4+}) so that the average oxidation state of nickel in γ-phase would be 3.5 or higher. Therefore the specific discharge capacity beyond the theoretical value of 289 mAh g^{-1} can be observed [29–31]. The observation of the excess discharge capacity is an indication of the formation of γ-NiOOH, which results from overcharge or floating phenomena of the electrode. Even though the formation of γ-NiOOH leads to high discharge capacity, but it results in significant volume expansion or swelling of the electrode, which adversely affects the effective contact between particles of active materials and thus increases the resistance of the electrode reaction and leads to faster capacity decay, especially at high-rate or high-temperature charge–discharge [23]. So prohibition of γ-NiOOH formation will be favorable for higher utilization efficiency of the active materials and longer cycling stability of the electrode. Our β-$Ni(OH)_2$/Ni-foam electrode shows a specific discharge capacity close to but less than the theoretical value corresponding to the reduction of β-NiOOH to β-$Ni(OH)_2$ shown in Eq. (1). This suggests that γ-NiOOH is unlikely formed during the charge–discharge process. Recently, it has been reported that when β-$Ni(OH)_2$ nanosheets were organized to form a carnation-like morphology, the formation of γ-NiOOH could be restrained [28].

Nickel hydroxide particles with diverse shapes and dimensions have been evaluated as the positive electrode material of rechargeable alkaline batteries via galvanostatic discharge tests to measure their specific capacities. It was found that crystallite size, morphology, porosity, and other physicochemical parameters apparently

affect the specific discharge capacity of β-Ni(OH)$_2$. Nano-sized nickel hydroxides usually display higher discharge capacity than micro-sized ones. For example, Cai et al. [12] found that β-Ni(OH)$_2$ nanotubes with a wall thickness of 20–30 nm and ~60 μm long displayed a highest discharge capacity of 315 mAh g^{-1} at 50 mA g^{-1}. Similar results have been obtained by Li et al. [29]. They demonstrated that β-Ni(OH)$_2$ nanotubes with a thickness of 20–30 nm and an average outer diameters of ~200 nm have achievable discharge capacity of 315 mAh g^{-1} at 50 mA g^{-1}. Both Cai and Li attributed the excess capacity over the theoretical value to the partial formation of γ-NiOOH. Sakai et al. [32] found that β-Ni(OH)$_2$ hexagonal nanosheets of 30–40 nm average thickness and ~2 μm diameter showed a specific discharge capacity of 219.5 mAh g^{-1} at a discharge rate of 0.2 C. Both Cai et al. [12] and Han et al. [4] demonstrated that commercial micrometer grade spherical β-Ni(OH)$_2$ powders has a specific discharge capacity of ~265 mAh g^{-1} at 50 mA g^{-1}. Tao et al. [33] found that Ni(OH)$_2$ microtubes with the length, wall thickness and outer diameter of 10–40, 0.5–1.5 and 2–4 μm, respectively, displayed a highest discharge capacity of 232.4 mAh g^{-1} at 80 mA g^{-1}. So the specific discharge capacity of our β-Ni(OH)$_2$ directly grown on Ni-foam current collector (275 mAh g^{-1}) is lower than that of β-Ni(OH)$_2$ nanotubes powder (315 mAh g^{-1}), but higher than that of nanosheets (219.5 mAh g^{-1}), commercial micrometer grade spherical powders (265 mAh g^{-1}) and microtubes (232.4 mAh g^{-1}).

It should be noted that conventional Ni(OH)$_2$ electrodes are generally fabricated by mixing Ni(OH)$_2$ powder with conducting carbons and polymer binders, and applying the paste to Ni foam current collector. Such obtained electrodes usually suffer drawbacks of low active material utilization due to presence of inaccessible regions to the electrolyte solution and poorly controlled porous structure, which limited the mass transport of reactants within the electrode. In this work, spherical clusters (~10 μm in diameter) of β-Ni(OH)$_2$ nanosheets (~60 nm in thickness) composed of nanoparticles (~20 nm in diameter) were directly attach to the skeleton of nickel foam current collector. The obtained electrode has the advantages: (1) conducting carbons and binders are not needed; (2) Ni(OH)$_2$ has high utilization efficiency because all Ni(OH)$_2$ particles are in electrical contact (directly or indirectly through other particles) with current collector; (3) the Ni(OH)$_2$ spheres have porous structure and a large surface area. The open spaces within β-Ni(OH)$_2$ spheres allow for easy penetration of electrolyte into the inner region of the electrode and can accommodate expansion of the electrode; (4) traditionally, Ni(OH)$_2$ electrodes were prepared in two steps, the preparation of Ni(OH)$_2$ powder and the fabrication of Ni(OH)$_2$–carbon-binder electrode. The preparation of our β-Ni(OH)$_2$/Ni-foam electrodes combined the two step together and realized one-step preparation of Ni(OH)$_2$ electrode. So our method is relatively simple comparing to conventional methods and it also uses readily available low cost raw materials.

3.3. Performance of Ni(OH)$_2$/Ni-foam positive electrode in a Ni–MH battery

To evaluate the performance of Ni(OH)$_2$/Ni-foam as the positive electrode of Ni–MH batteries, a prototype Ni–MH battery was assembled using Ni(OH)$_2$/Ni-foam as the positive electrode. The negative electrode contained excess amount of hydrogen storage alloy. The battery was repeatedly charged and discharged at 1 C (refer to β-Ni(OH)$_2$) at ambient temperature. Fig. 6 shows the typical charge–discharge curves in the first cycle and Fig. 7 shows the cycling performance of the battery. The specific capacity and the coulombic efficiency are evaluated for β-Ni(OH)$_2$). As seen from Fig. 6, when the battery is charged at 1 C to a cutoff voltage of 1.45 V and then discharged at 1 C to 0.9 V, the specific discharge

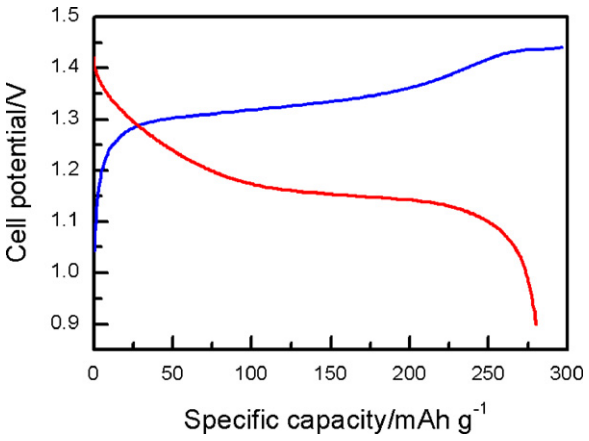

Fig. 6. Charge–discharge curves of the Ni–MH battery with Ni(OH)$_2$/Ni-foam positive electrode measured at 1 C and room temperature.

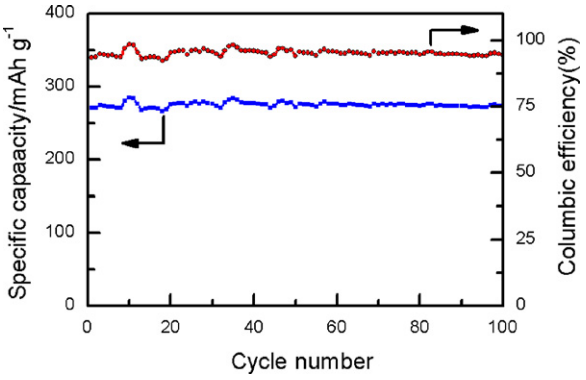

Fig. 7. Cycling performance of the Ni–MH battery with Ni(OH)$_2$/Ni-foam positive electrode measured at 1 C charge–discharge condition.

capacity for β-Ni(OH)$_2$ reaches 280 mAh g^{-1}. The discharge plateau voltage (around 1.15 V) is, however, slightly lower than the typical value of a Ni–MH battery (1.2 V). This may be caused by the low electronic conductivity of Ni(OH)$_2$/Ni-foam positive electrode due to the thick Ni(OH)$_2$ layer (~10 μm). The conductivity of Ni(OH)$_2$ layer might be improved by the addition of Co [29,34]. The investigations are undergoing in our laboratory. During the period of 100 charge–discharge cycles at 1 C, the discharge specific capacity of β-Ni(OH)$_2$ fluctuates between 284 mAh g^{-1} and 270 mAh g^{-1}. The coulombic efficiency ranges from 92.2% to 98.5%. These results demonstrate that the Ni(OH)$_2$/Ni-foam positive electrode has superior cycling stability at high charge–discharge rates.

4. Conclusions

A facile one-step method for the preparation of nickel foam supported β-Ni(OH)$_2$ nanosheets electrode was demonstrated. β-Ni(OH)$_2$ nanosheets wrap together to form spherical clusters and directly attach to the skeletons of nickel foam, which serves as the current collector of the electrode. The use of ancillary conducting materials and binders was eliminated. The nanosheets have porous structure giving the electrode a large surface area. The open spaces within β-Ni(OH)$_2$ allow for easy penetration of electrolyte into the inner region of the electrode and can accommodate expansion of the electrode. Each nanosheet is in electrical contact with other nanosheets and ultimately in contact with the nickel foam current collector, which ensures high utilization of β-Ni(OH)$_2$. The obtained electrode exhibits a specific capacity of 284 mAh g^{-1} at 1 C discharge rate and superior cycling stability. Considering the easy

and economic fabrication and high rate performance, β-Ni(OH)$_2$ nanosheets electrodes supported by nickel foam will hold promise for improved performance of Ni–MH batteries.

Acknowledgements

We gratefully acknowledge the financial support of this research by National Nature Science Foundation of China (20973048) and Harbin Engineering University (HEUFT08008).

References

[1] M.A. Fetcenko, S.R. Ovshinsky, B. Reichman, K. Young, C. Fierro, J. Koch, A. Zallen, W. Mays, T. Ouchi, J. Power Sources 165 (2007) 544.
[2] G.A. Snook, N.W. Duffy, A.G. Pandolfo, J. Power Sources 168 (2007) 513.
[3] S. Deabate, F. Fourgeot, F. Henn, Electrochim. Acta 51 (2006) 5430.
[4] X.J. Han, P. Xu, C.Q. Xu, L. Zhao, Z.B. Mo, T. Liu, Electrochim. Acta 50 (2005) 2763.
[5] D.E. Reisner, A.J. Salkind, P.R. Strutt, T.D. Xiao, J. Power Sources 65 (1997) 231.
[6] X. Wang, H. Luo, P.V. Parkhutik, A.C. Millan, E. Matveeva, J. Power Sources 115 (2003) 153.
[7] E. Shangguan, Z. Chang, H. Tang, X.-Z. Yuan, H. Wang, Int. J. Hydrogen Energy 35 (2010) 9716.
[8] W. Zhang, W. Jiang, L. Yu, Z. Fu, W. Xia, M. Yang, Int. J. Hydrogen Energy 34 (2009) 473.
[9] H.S. Kim, T. Itoh, M. Nishizawa, M. Mohamedi, M. Umeda, I. Uchida, Int. J. Hydrogen Energy 27 (2002) 295.
[10] K. Matsui, T. Kyotani, A. Tomita, Adv. Mater. 14 (2002) 1216.
[11] Z.H. Liang, Y.J. Zhu, X.L. Hu, J. Phys. Chem. B 108 (2004) 3488.
[12] F.S. Cai, G.Y. Zhang, J. Chen, X.L. Gou, H.K. Liu, S.X. Dou, Angew. Chem. 116 (2004) 4308.
[13] Y. Tan, S. Srinivasan, K.S. Choi, J. Am. Chem. Soc. 127 (2005) 3596.
[14] C. Coudun, J.F. Hochepied, J. Phys. Chem. B 109 (2005) 6069.
[15] D. Yang, R. Wang, J. Zhang, Z. Liu, J. Phys. Chem. B 108 (2004) 7531.
[16] D. Yang, R. Wang, M. He, J. Zhang, Z. Liu, J. Phys. Chem. B 109 (2005) 7654.
[17] M. Cao, X. He, J. Chen, C. Hu, Cryst. Growth Des. 7 (2006) 170.
[18] Y. Li, B. Tan, Y. Wu, Chem. Mater. 20 (2008) 567.
[19] Y. Li, B. Tan, Y. Wu, J. Am. Chem. Soc. 128 (2006) 14258.
[20] G.L. Wang, D.X. Cao, C.L. Yin, Y.Y. Gao, J.L. Yin, L. Cheng, Chem. Mater. 21 (2009) 5112.
[21] Y.Y. Gao, S.L. Chen, D.X. Cao, G.L. Wang, J.L. Yin, J. Power Sources 195 (2010) 1757.
[22] A.A. Kamnev, Electrochim. Acta 41 (1996) 267.
[23] D. Singh, J. Electrochem. Soc. 145 (1998) 116.
[24] P. Haring, R. Kotz, J. Electroanal. Chem. 385 (1995) 273.
[25] D.B. Kuang, B.X. Lei, Y.P. Pan, X.Y. Yu, C.Y. Su, J. Phys. Chem. C 113 (2009) 5508.
[26] W.K. Hu, X.P. Gao, D. Noréus, T. Burchardt, N.K. Nakstad, J. Power Sources 160 (2006) 704.
[27] A.B. Beleke, M. Mizuhata, J. Power Sources 195 (2010) 7669.
[28] L.X. Yang, Y.J. Zhu, H. Tong, Z.H. Liang, W.W. Wang, Cryst. Growth Des. 7 (2007) 2716.
[29] W. Li, S. Zhang, J. Chen, J. Phys. Chem. B 109 (2005) 14025.
[30] H. Bode, K. Dehmelt, J. Witte, Electrochim. Acta 11 (1966) 1079.
[31] G. Sakai, M. Miyazaki, T. Kijima, J. Electrochem. Soc. 157 (2010) A932.
[32] G. Sakai, M. Miyazaki, T. Kijima, J. Electrochem. Soc. 157 (2010) A480.
[33] F. Tao, M. Guan, Y. Zhou, L. Zhang, Z. Xu, J. Chen, Cryst. Growth Des. 8 (2008) 2157.
[34] P. Elumalai, H.N. Vasan, N. Munichandraiah, J. Power Sources 93 (2001) 201.